Article

Applied Spectroscopy

www.s-a-s.org

Applied Spectroscopy
2019, Vol. 73(1) 59–66

DOI: 10.1177/0003702818797959
journals.sagepub.com/home/asp
SAGE

Characterization of Oxide Layers on Technical Copper Material Using Ultraviolet Visible (UV–Vis) Spectroscopy as a Rapid On-Line Analysis Tool

Jan Stiedl[1,2,3], Simon Green[3], Thomas Chassé[1,4], and Karsten Rebner[2]

Abstract

An ultraviolet visible (UV–Vis) spectroscopy method was developed that can quantitatively characterize a technical copper surface to determine oxide layers and organic impurities. The oxide layers were produced by a heating step at 175 °C for four different times (range = 1–10 min). Partial least squares (PLS) regression was used to establish a relation between the UV–Vis spectra and film thickness measurements using Auger electron spectroscopy depth profiles. The validation accuracy of the regression is in the range of approximately 2.3 nm. The prediction model allowed obtaining an estimation of the oxide layer thickness with an absolute error of 2.9 nm. Alternatively, already known methods cannot be used because of the high roughness of the technical copper surfaces. An integrating sphere is used to measure the diffuse reflectance of these surfaces, providing an average over all angles of illumination and observation.

Keywords

Oxide layer, copper, ultraviolet visible, UV–Vis spectroscopy, on-line, multivariate, Auger electron spectroscopy

Date received: 30 April 2018; accepted: 6 August 2018

Introduction

The potentially high volumes and extreme performance demands of the hybrid and electric automotive market will strongly influence the packaging of power modules. Over the past several years, conventional packaging in an aluminum box was replaced with direct packaging with an epoxide mold compound. The reliability of direct packaging relies on adhesion between the copper leadframe and the packaging material. In turn, the adhesiveness of the epoxy polymer is correlated with the oxidation time of the copper leadframes. Adhesion increases until the oxide layer reaches a critical thickness.[1–5] However, the duration of oxidation is set to produce an oxide layer with a thickness considerably lower than the critical value given the difficulty in measuring the oxide-layer thickness during oxidation.

The oxidation of copper has been the focus of extensive research over the past several years. In addition to the formation and thickness of native oxide layers,[6–8] the kinetics of the oxidation of copper at different temperatures has been investigated. Studies based on the oxidation of crystals well describe the kinetics of oxidation in the temperature range of 25–350 °C.[9–12] The kinetics of copper oxidation at higher temperatures is more often investigated using film samples at temperatures as high as 1200 °C.[13–18] In addition to kinetics, the influence of oxidation on adhesion has been frequently investigated in recent years.[19–22]

Standard techniques such as X-ray photoelectron spectroscopy, Auger electron spectroscopy (AES), and time-of-flight secondary ion mass spectrometry (TOF-SIMS) cannot be used to measure the oxide-layer thickness during the manufacturing process because of the required

[1]University of Tubingen, Institute of Physical and Theoretical Chemistry, Tubingen, Germany
[2]Reutlingen University, Process Analysis and Technology, Reutlingen, Germany
[3]Robert Bosch GmbH, Automotive Electronics, Reutlingen, Germany
[4]Center for Light-Matter Interaction, Sensors & Analytics (LISA+), Tuebingen, Germany

Corresponding author:
Karsten Rebner, Reutlingen University, Process Analysis & Technology, Alteburgstrasse 150, 72762 Reutlingen, Germany.
Email: karsten.rebner@reutlingen-university.de

ultra-high vacuum and limited dimensions of the samples. Moreover, the extreme roughness of technical surfaces limits the application of certain measurement techniques, such as interferometry, sequential electrochemical reduction analysis, and infrared reflection techniques.[23–26]

Ultraviolet visible (UV–Vis) diffuse reflection methods represent a potential rapid online approach to measuring oxide-layer thickness. This technique can reveal transitions of Cu_2O and CuO in the UV range corresponding to visible-range color changes of the substrate during oxidation. These effects can be attributed to light interference. Light is refracted if it penetrates a thin film such as a copper oxide film. Reflection, which is dependent on film thickness, can then be calculated with the common Fresnel equations with the refractive index of the first layer, n_1, and the second layer, n_2, and the angle of the incident light, Θ. The fraction of the incident power reflected at the interface is given by the reflectance *R* and can be calculated with the following equations.[27]

The reflectance for s-polarized light is given by

$$R_s = \left| \frac{n_1 \cos\Theta_i - n_2 \sqrt{1 - \left(\frac{n_1}{n_2}\sin\Theta_i\right)^2}}{n_1 \cos\Theta_i + n_2 \sqrt{1 - \left(\frac{n_1}{n_2}\sin\Theta_i\right)^2}} \right|^2 \quad (1)$$

whereas the reflectance for p-polarized light is given by

$$R_p = \left| \frac{n_1 \sqrt{1 - \left(\frac{n_1}{n_2}\sin\Theta_i\right)^2} - n_2 \cos\theta_i}{n_1 \sqrt{1 - \left(\frac{n_1}{n_2}\sin\Theta_i\right)^2} + n_2 \cos\theta_i} \right|^2 \quad (2)$$

If the incident light is unpolarized, the reflectance is

$$R = \frac{1}{2}(R_s + R_p) \quad (3)$$

When light makes multiple reflections between two or more parallel surfaces, the multiple beams of light generally interfere with one another, resulting in net transmission and reflection amplitudes that depend on the light's wavelength. The interference, however, is observed only when the surfaces are at distances comparable to or smaller than the light's coherence length, which, for ordinary white light is a few micrometers

In the present work, the thicknesses of oxide layers are quantified through multivariate data analysis. Auger electron spectroscopy depth profiles are used to construct a partial least squares (PLS) regression model for the measurement of oxide-layer thicknesses. The results are then correlated with those obtained through other techniques.

Materials and Experimental Procedure

Sample Preparation

Oxygen-free extra low phosphorus Cu (Cu-PHC) samples (Wieland-Werke AG; Wieland-K14; Cu $\geq$ 99.95%; $P \approx 0.003\%$) with dimensions of $2.1 \times 4.9 \times 0.3$ cm were used. The samples were cleaned with Zestron Vigon A 200 for 6 min, rinsed twice with deionized water for 2 min, and dried under N_2 gas. Oxidation was performed on a heating plate (Gerhardt Bonn H-22) at 175 °C for 0, 1, 2, 5, or 10 min in air under atmospheric pressure. The temperature was monitored with a testo 735-type 18-temperature probe. These parameters are representative of those used during the actual device fabrication process.

Surface Treatments

The surfaces of the samples were milled with a Mapal DMG-DMC650V equipped with a HSK63 spindle. The milling head had a diameter of ø100 mm and 14 blades. The cutting speed was set to 1000 m/min at a feed rate of 4660 mm/min.

Methods

Roughness Measurements. Roughness measurements were performed with a CyberScan Vantage 2 (Cybertechnologies) equipped with a P-CHR-600 probe. Surface scanning parameters were set to 2000×2000 μm with a step width of 5 μm.

Scanning Electron Microscopy Energy-Dispersive X-ray Spectroscopy. Energy-dispersive X-ray spectroscopy (EDX) measurements were conducted on a HITACHI SU8030 field-emission scanning electron microscope. The EDX spectra were acquired at an accelerating voltage of 5 kV.

Raman Spectroscopy. Oxidized samples were analyzed by Raman spectroscopy using a confocal Raman spectrometer (LabRam HR800) equipped with a BX 41 microscope (Horiba Jobin Yvon). A long-distance lens with 50× magnification and a numerical aperture of 0.75 were used. Spectra were recorded in backscattering geometry using a frequency-doubled neodymium-doped yttrium aluminum garnet (Nd:YAG) laser (30 mW) with an excitation wavelength of 532 nm.

Auger Electron Spectroscopy. Auger measurements were performed using Perkin Elmer PHI-600 equipped with Perkin Elmer 04-303 differential ion gun. Instrumental parameters consisted of a 3.0 keV electron beam voltage and a 1.3 electron beam current. Sputtering was conducted with Ar^+ ions at 3.35 keV and 8 μA on an area of 0.1 cm^2 incident to 30° with respect to the sample surface normal. The chamber pressure was 3.0×10^{-8} mbar. Calibration was conducted with an Si/SiO_2 standard and an Si wafer with an evaporated Cu film.

Ultraviolet Visible Spectroscopy. The UV–Vis spectra were collected using an Ocean Optics Flame-S-UV/VIS-ES spectrophotometer equipped with a DH-2000-BAL light source and an ISP-30-6 integrating sphere. Sample absorption was measured in the wavelength range of 200–800 nm. The SCOUT 98 software was used to simulate spectra. Required values were taken directly from the software and cross-referenced with experimental values reported by Karlsson et al.[21]

Software for Multivariate Analysis. The Unscrambler X version 10.4.45271.25 from Camo Software with NIPALS algorithm was used to calculate the PLS. Systematic cross validation (123123, with 20 segments) was conducted.

Results and Discussion

Oxidized Cu samples were investigated using UV–Vis diffuse reflectance spectroscopy. Spectra are shown for different steps of the oxidation process in Fig. 1a. The initial spectrum representing Cu with a native oxide film is similar to those reported in the literature.[28–30] A band at 350 nm arises with increasing oxide-layer thickness. Additionally, a band at 580 nm becomes visible in the spectra recorded from samples with the highest oxide-layer thicknesses. These two bands have different origins. The band at 350 nm is due to thin-film interferences, which arise from the changes in the refractive index from air to copper oxide and to copper.

Spectra were simulated for comparison with experimental data. The refractive indices of copper oxides have been provided by Karlsson et al.,[21] that of bare copper by Johnson et al.,[31] and that of air by Ciddor.[32]

First, the reflectance due to the interfaces, air/oxide/metal, was calculated using Eqs. 1 and 2. The Fresnel equations were used to calculate transmission, which is dependent on layer thickness.[21] The SCOUT 98 software[33] was used to simulate the spectra corresponding to different oxides and different incidence angles. Results of the simulations for CuO and Cu_2O films are shown in Fig. 1b–d.

The experimental and theoretical spectra of oxide layers with low thicknesses (11 nm) are in rather good agreement,

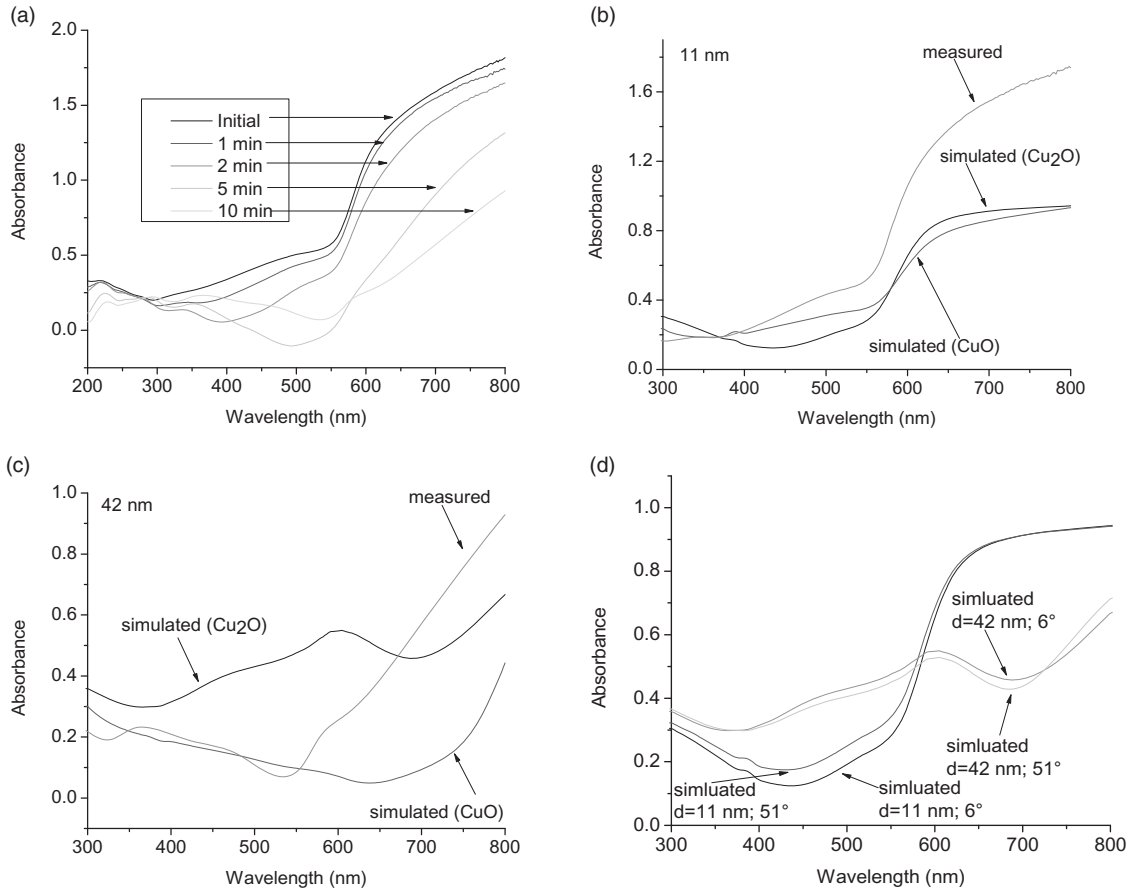

Figure 1. (a) Ultraviolet visible diffuse reflectance spectra of samples oxidized for different durations; comparison of the experimental and simulated UV–Vis absorbance spectra acquired at layer thicknesses of (b) 11 nm and (c) 42 nm; (d) comparison of simulated spectra corresponding to different angles of incident light.

as shown in Fig. 1b. The remaining small differences among spectra are attributed to the surface roughness and scattering of the incident light beam. On the other hand, there is only slight agreement regarding the thicker oxide layer of 42 nm, as shown in Fig. 1c. This seems to be mainly due to superimposed interference and absorption effects.[34] The latter effects are not directly included in this theoretical model.

In order to assign possible remaining differences in Fig. 1b and 1c, the surface roughness was measured to evaluate the incidence angle of light. The results are shown in Fig. 2. The topology of the samples is dominated by striae, which were produced during milling of the Cu plates. The typical height of the striae is approximately 2–3 μm, much larger than the expected oxide film thickness.

For the first approximation, the surface structure can be assumed to be a sine wave. In the case of an assumed sinusoidal slope, the incidence angle may change between 51° and 6°, where the latter corresponds to the incidence angle to the surface normal given by the integrating sphere and the former would then be observed at the maximum slope of the sinusoidal surface roughness. In order to compare these two different incidence angles, we varied the angle in this range, as shown in Fig. 1d. At a high angle, intensity decreases and the positions of the peaks shift to shorter wavelengths. However, when considering the simulated and experimental spectra, bands in the measured spectra are blurred by shifts. This difference and the second visible peak at 580 nm in Fig. 1a are attributed to the absorbance of oxides.[35] The band gap of 2.2 eV for copper(I) oxide (Cu_2O)[36] results in absorption at 564 nm, which matches the peak at 580 nm in the experimental spectra. The band gap of 1.2 eV for copper(II) oxide (CuO)[37] is related to an absorption at 1033 nm, which is not within the wavelength range investigated in the present work. Spectra reported by Messaoudi et al.[38] for Cu_2O and by Khaorapapong[39] for CuO also show these two peaks.

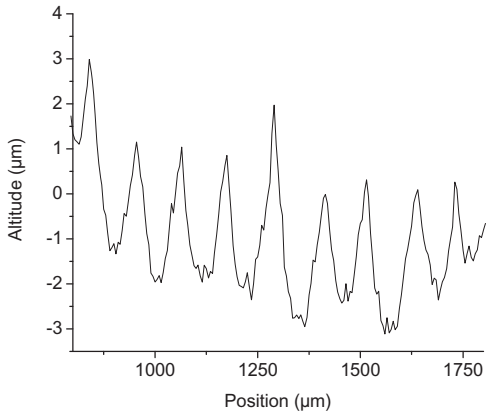

Figure 2. Roughness measurements acquired with a step size of 1 μm.

Appearance of absorption features and the large sample size preclude the evaluation of oxide-layer thickness through conventional methods. Interference only accounts for oxide layers with low thicknesses. The spectra of oxide layers with high thicknesses exhibit overlapping absorbance features. Nevertheless, interference features in the spectra of oxide layers with low thicknesses are too weak to enable the determination of film thickness on the basis of minima or maxima positions. Hut et al. reported that measurable interference can only be produced at high temperatures and after a long oxidation time.[35] Thus, oxide-layer thicknesses were measured through AES depth profiling to obtain reference data. A schematic AES depth profile of a sample oxidized for 10 min and the corresponding survey spectra are shown in Fig. 3.

The sample surface is covered with a thin carbon contamination layer, which is a consequence of processing under normal atmospheric conditions. A peak at 269.5 eV is present, known as the C KVV Auger peak.[40] In addition to these peaks, peaks from oxygen KVV are observed at 514.5 eV[40,41] and the main copper LMM peak is observed at

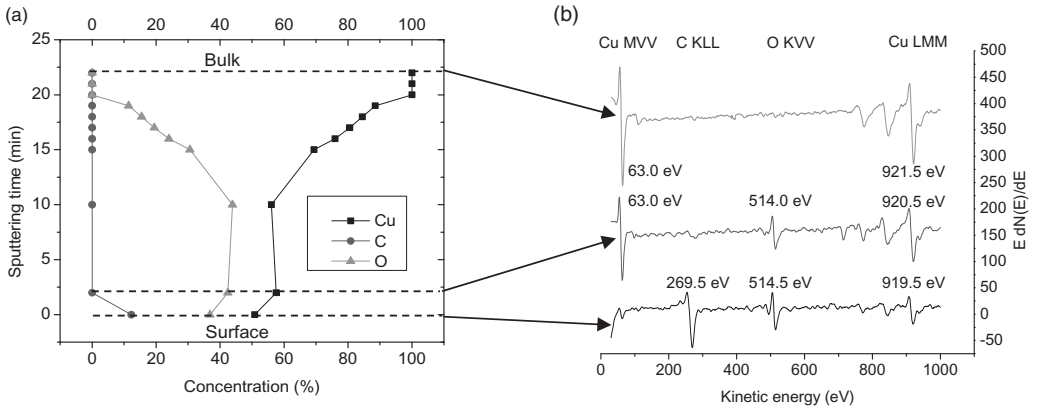

Figure 3. Auger electron spectroscopy depth profile and corresponding survey spectra of a sample oxidized for 10 min at 175 °C.

919.5 eV.[42] After 2 min of sputtering, the top layers are removed and carbon peaks are no longer visible in the spectra. Consequently, the surface-sensitive low-energy Auger peak of copper remains at 63 eV.[43]

The peak ratio between copper and oxygen remains stable to a depth of 22.5 nm, or 10 min of sputtering. The oxygen concentration in the next few layers decreases to zero after 20 min of sputtering, or a depth of 45.0 nm. The shift of the copper LMM peak to a lower kinetic energy from the surface layer to the bulk material is due to the change of oxidation state.[40–42,44] Thus, CuO dominates the spectrum of the surface layer and peaks attributed to a mixture of CuO and Cu_2O appear in the spectrum of the near-surface layer. In the spectrum of the bulk material, the position of the copper LMM peaks indicates that only metallic copper exists in the bulk material. Therefore, the oxygen signal disappears from the spectrum. All depth profiles exhibit the same development, which is dependent on oxidation time and, thus, oxide-layer thickness. Table I shows the results of all AES depth profiles, which are comparable with those reported in the literature.[24,41,45–47] An additional group of oxide films with different thicknesses is present because of the inhomogeneous oxidation of copper. The samples within this group partially derive from oxidation treatments for 5 or 10 min.

Table I. Results of the AES depth profiles.

Oxidation time (min)	Average layer thickness (nm)	Standard deviation (nm)
1	4.50	0.0
2	10.6	0.8
5	28.7	1.3
5 and 10	35.0	1.0
10	41.4	0.3

For the creation of the different groups the AES result were used to obtain good cluster selections.

We used PLS regression to derive complementary information about the oxide-layer thickness from all 142 of the experimentally acquired UV–Vis spectra. This approach enables us to obtain the regression of the AES depth profiles and the UV–Vis spectra.

To define small changes in spectra, a derivation with nine-point Savitzky–Golay smoothing was performed. The model was calibrated using systematic full cross-validation. The scores and the loadings of the first three latent variables (LVs) are shown in Fig. 4. The PLS model needs three factors to minimize calibration and validation error for the present set of samples.

The scores of different sample types are well discriminated. Every group of samples with a corresponding oxide thickness appears as a sharp cluster. The scores of the initial samples are located at the origin of all three score values. At the beginning of oxidization, clusters move toward high LV-1, LV-2, and LV-3 scores. Their shift across scores appears as a helix as a result of the pronounced ranges of the regression coefficients, RC. Three different wavelength regions are recognized (Fig. 4): The first range of 220–300 nm and the third range of 500–600 nm are strongly correlated. Comparing these ranges with those of the original spectra (Fig. 1a) reveals that these ranges are correlated with highly oxidized samples. By contrast, the second wavelength range of 300–450 nm is strongly correlated with weakly oxidized samples. For the calculation of the oxide layer thickness, d, by using the PLS model, the B(0) and the regression coefficient of the third LV is needed. The following calculation is done by a standard linear regression using B(0) as the intercept and the regression coefficient, RC, and the spectra as the slope.

$$d\,[nm] = 18.75 + I_{200} \cdot RC_{200} + I_{201} \cdot RC_{201} + \cdots + I_{800} \cdot RC_{800} \quad (4)$$

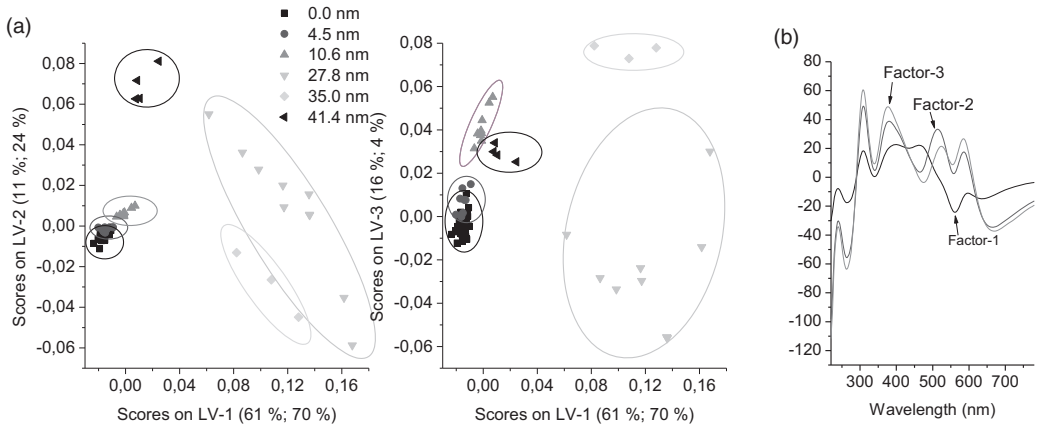

Figure 4. (a) Scores of the PLS model in the space of the first, second, and third latent variable plotted against each other. (b) Regression coefficients of the first three latent variables of the PLS model for oxide-layer thickness. B(0) = 18.75; factor 3.

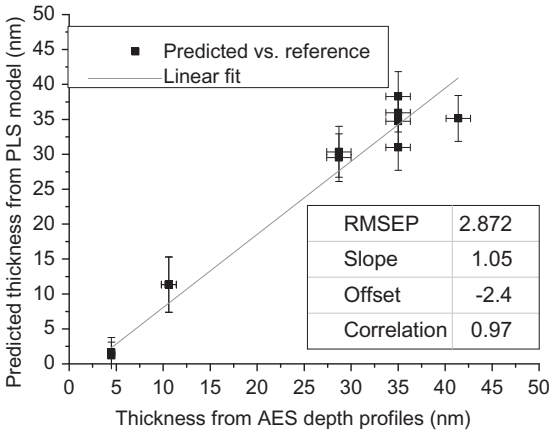

Figure 5. Values of the oxide-layer thickness calculated using the PLS model and using the AES depth profile results.

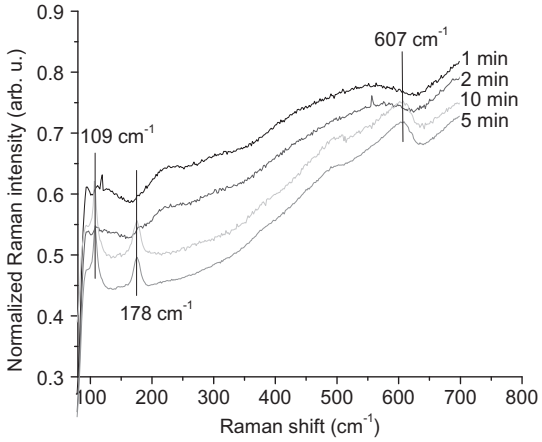

Figure 6. Raman spectra of oxidized copper samples.

The PLS model describes 88% of the UV–Vis data and 98% of the oxide-layer thickness data with three factors. When the number of LVs is increased to four, the explained variance of the UV–Vis data and the variance of the oxide-layer thickness increases to 96% and 99%, respectively. However, the use of four factors is not recommended because of the limited availability of information about *Y*-variables. For evaluating the robustness of the PLS model, the root mean square error of calibration (RMSEC) and the root mean square error of validation (RMSECV) are calculated according the literature.[48] The RMSEC and RMSECV are 2.0 and 2.3 nm, respectively. The bias for the validation is –0.060.

Comparing the aforementioned values with the variation of oxide-layer thicknesses revealed a relative error of 4.5% for calibration and 5.1% for validation. These results indicate that the PLS model can well describe UV–Vis spectra and, therefore, can be used to derive oxide-layer thicknesses. A set of 11 samples which were not used for model calibration or validation before were instead applied for prediction and model verification. The predicted oxide-layer thicknesses versus the corresponding values measured by AES depth profiles were displayed against each other and a linear fit was performed (Fig. 5). First, the coefficient of determination of 0.970 indicates that the linear fit described by the PLS model is acceptable. A perfect model with ideal samples has an intercept value of 0 and a slope of 1. In this case, the intercept value is −2.40 given that the homogeneity of the initial samples did not satisfy the model. The value for the slope is 1.05 and is considered satisfactory. Second, the root mean square error of prediction (RMSEP) for the prediction is 2.9 nm, which is an acceptable value applied to the RMSECV.

Raman and SEM-EDX measurements were carried out and the results were compared with those of the PLS model and with the AES depth profiles. The Raman spectra, which are shown in Fig. 6, provide complementary information about the oxide films. The top layer lacks signals from carbon contamination, indicating low sensitivity regarding these compounds. The spectrum of the sample oxidized for 1 min does not exhibit a substantial oxide signal. The intensities of the copper-oxide-related Raman peaks begin to increase after the initial oxidation steps, beginning in the spectrum of the sample oxidized for 2 min. A shoulder at 109 cm^{-1} is present. The spectra of other samples oxidized for 5 and 10 min exhibit a strong signal in this region. Two other signals are present at 178 cm^{-1} and 607 cm^{-1}. All of the three detected signals belong to Cu_2O.[49,50] A signal from CuO, which would be located at 300 cm^{-1}, is absent.[50–52]

Table II. O/Cu ratios calculated from SEM-EDX measurements.

Oxidation time (min)	O/Cu signal	Standard deviation
1	0.0155	0.0022
2	0.0183	0.0019
5	0.0397	0.0073
10	0.0421	0.0026

Oxygen K X-ray signals were normalized to the copper L emission signal for the evaluation of SEM-EDX results. The results are shown in Table II. The ratio between the oxygen and copper signals is correlated with the oxidation time and increases with increasing copper oxide layers.

Figure 7 was generated to summarize all of the results and compare the used measurement techniques. It shows the total normalized Raman peak intensities, the normalized intensity ratio between oxygen and copper peaks from EDX, and the oxide-layer thickness as a function of the oxidation time. All of these results indicate the same relative growth of oxide layers. This agreement is strong evidence for the correctness of the calibrated results. However,

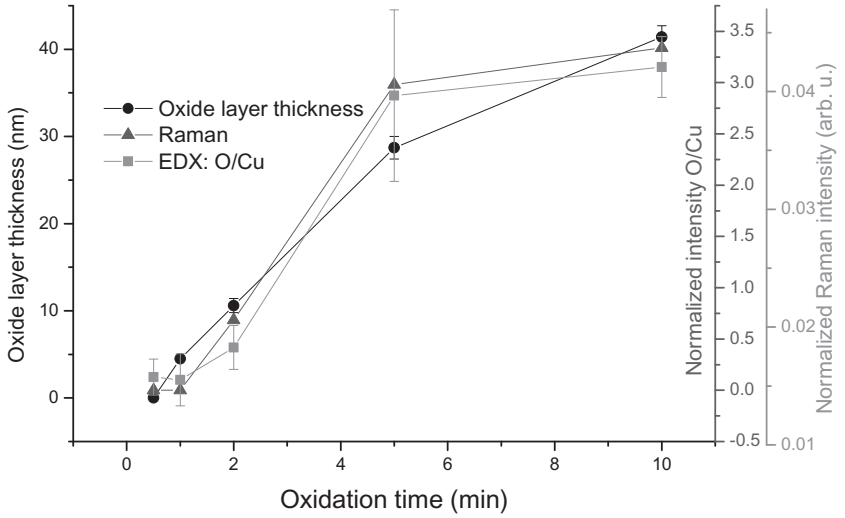

Figure 7. Combined plot of oxide-layer thickness measurements, normalized EDX intensity of the oxygen-to-copper peak ratio, and the peak height in Raman spectra.

SEM-EDX and Raman measurements are insufficient for the analysis of oxide-layer thickness in the researched range. Instead, the PLS model for UV–Vis spectroscopy is needed to measure the oxide layer thickness.

Conclusion

This study introduces an alternative novel approach for the thickness measurement of copper oxide films. The proposed approach combines UV–Vis absorbance measurements and multivariate data. The simultaneous use of interference and absorbance spectra increases measurement accuracy. Equipment setup and data evaluation enable the measurement of extremely rough samples. Previously, state-of-the-art techniques could not be applied for the measurement of even slightly uneven surfaces.

The proposed method enables the measurement of oxide-layer thickness during the manufacturing process. Thus, the direct packaging of power modules can be tuned using surfaces produced through traditional methods. In addition, process windows can be enlarged if the exact critical process parameters are known.

Universally available equipment and operating conditions enable the application of the proposed measurement system in other branches of industry, such as the battery industry, wherein copper is commonly used as an electrode material and oxide surface layers are critical components.

Conflict of Interest

The authors report there are no conflicts of interest.

Funding

The authors received no financial support for the research, authorship, and/or publication of this article.

ORCID iD

Jan Stiedl http://orcid.org/0000-0001-5553-8631

References

1. S.J. Cho, K.W. Paik, Y.G. Kim. "The Effect of the Oxidation of Cu-Base Leadframe on the Interface Adhesion Between Cu Metal and Epoxy Molding Compound". IEEE Trans. Compon., Packag. Manuf. Technol. 1997. 20(2): 167–175.
2. B.H. Moon, H.Y. Yoo, K. Sawada. "Optimal Oxidation Control for Enhancement of Copper Lead Frame-EMC Adhesion in Packaging Process". Proceedings of the 48th Annual Electronic Components and Technology Conference (Cat. No. 98CH36206). Seattle, WA; 25–28 May, 1998.
3. R. Berriche, S.C. Vahey, B.A. Gillet. "Effect of Oxidation on Mold Compound-Copper Leadframe Adhesion". Proceedings International Symposium on Advanced Packaging Materials. Processes, Properties and Interfaces (IEEE Cat. No. 99TH8405). Braselton, GA; 14–17 March, 1999.
4. T.G. Kang, I.S. Park, J.H. Kim, K.S. Choi. "Characterization of Oxidized Copper Leadframes and Copper Epoxy Molding Compound Interface Adhesion in Plastic Package". Proceedings of 3rd International Conference on Adhesive Joining and Coating Technology in Electronics Manufacturing 1998 (Cat. No. 98EX180). Binghamton, NY; 30 September, 1998.
5. R. Berriche, R. Lowry, M.I. Rosenfield. "An Oxidation Study of Cu Leadframes". Proceedings International Symposium on Advanced Packaging Materials. Processes, Properties and Interfaces (IEEE Cat. No. 99TH8405). Braselton, GA; 14–17 March, 1999. Pp. 275–281.
6. A. Manara, V. Sirtori, L. Mammarella. "Optical Ellipsometry and Electron Spectroscopy Studies of Copper Oxidation Related to Copper on Printed Circuit Boards". Surf. Interface Anal. 1992. 18(1): 32–38.
7. H. Derin, K. Kantarli. "Optical Characterization of Thin Thermal Oxide Films on Copper by Ellipsometry". Appl. Phys. A: Mater. Sci. Process. 2002. 75(3): 391–395.
8. M. Ramirez, L. Henneken, S. Virtanen. "Oxidation Kinetics of Thin Copper Films and Wetting Behaviour of Copper and Organic Solderability Preservatives (OSP) with Lead-Free Solder". Appl. Surf. Sci. 2011. 257(15): 6481–6488.
9. G.W. Poling. "Infrared Reflection Studies of the Oxidation of Copper and Iron". J. Electrochem. Soc. 1969. 116(7): 958–963.

10. X. Li, L. Li, Z. Ma, J. Lu, et al. "Boron Doping Effects on Microcrystalline Silicon Film Roughness Studied by Spectroscopic Ellipsometry". J. Alloys Compd. 2016. 684(5): 582–586.
11. I. Platzman, R. Brener, H. Haick, R. Tannenbaum. "Oxidation of Polycrystalline Copper Thin Films at Ambient Conditions". J. Phys. Chem. C. 2008. 112(4): 1101–1108.
12. J.W. Lim, J. Iijima, Y. Zhu, J.H. Yoo, et al. "Nanoscale Investigation of Long-Term Native Oxidation of Cu Films". Thin Solid Films. 2008. 516(12): 4040–4046.
13. P. Keil, D. Lützenkirchen-Hecht, R. Frahm. "Investigation of Room Temperature Oxidation of Cu in Air by Yoneda-XAFS". AIP Conf. Proc. 2006. 490–492.
14. G. Zhou, J.C. Yang. "Initial Oxidation Kinetics of Copper (1 1 0) Film Investigated by in Situ UHV-TEM". Surf. Sci. 2003. 531(1): 359–367.
15. A.T. Fromhold, M.H. Anderson. "Oxidation Kinetics of Epitaxial (100) Copper Films at 25 °C and 50 °C". Oxid. Met. 2004. 62(3-4): 237–272.
16. F.W. Young, J.V. Cathcart, A.T. Gwathmey. "The Rates of Oxidation of Several Faces of a Single Crystal of Copper as Determined with Elliptically Polarized Light". Acta Metall. 1956. 4(2): 145–152.
17. K. Fujita, D. Ando, M. Uchikoshi, K. Mimura, et al. "New Model for Low-Temperature Oxidation of Copper Single Crystal". Appl. Surf. Sci. 2013. 276(1): 347–358.
18. M. O'Reilly, X. Jiang, J.T. Beechinor, S. Lynch, et al. "Investigation of the Oxidation Behaviour of Thin Film and Bulk Copper". Appl. Surf. Sci. 1995. 91(1–4): 152–156.
19. Y. Wan, X. Wang, H. Sun, Y. Li, et al. "Corrosion Behavior of Copper at Elevated Temperature". Int. J. Electrochem. Sci. 2012. 7: 7902–7914.
20. G.K.P. Ramanandan, G. Ramakrishnan, P.C.M. Planken. "Oxidation Kinetics of Nanoscale Copper Films Studied by Terahertz Transmission Spectroscopy". J. Appl. Phys. 2012. 111: 12. doi: 10.1063/1.4729808.
21. B. Karlsson, C.G. Ribbing, A. Roos, E. Valkonen, et al. "Optical Properties of Some Metal Oxides in Solar Absorbers". Phys. Scr. 1982. 25(6A): 826–831.
22. H. Wieder, A.W. Czanderna. "The Oxidation of Copper Films to CuO0.67". J. Phys. Chem. 1962. 66(5): 816–821.
23. L. De Los Santos Valladares, D.H. Salinas, A.B. Dominguez, D.A. Najarro, et al. "Crystallization and Electrical Resistivity of Cu_2O and CuO Obtained by Thermal Oxidation of Cu Thin Films on SiO_2/Si Substrates". Thin Solid Films. 2012. 520(20): 6368–6374.
24. S.K. Lahiri, N.K. Waalib Singh, K.W. Heng, L. Ang, et al. "Kinetics of Oxidation of Copper Alloy Leadframes". Microelectron. J. 1998. 29(6): 335–341.
25. C.T. Chong, A. Leslie, L.T. Beng. "Investigation on the Effect of Copper Leadframe Oxidation on Package Delamination". Proceedings of the 45th Electronic Components and Technology Conference. Las Vegas, NV; 21–24 May, 1995.
26. H.Y. Lee, J. Yu. "Effects of Oxidation Treatments on the Fracture Toughness of Leadframe/Epoxy Interfaces". Mater. Sci. Eng. 2000. 277(1–2): 154–160.
27. E. Hecht. "The Propagation of Light". In: K. Flathman, M. Bortakur, V. Tiwari, editors. Optics. Harlow, UK: Pearson Education Limited, 2017. Chap. 4, Pp. 123–125.
28. M. Lenglet, K. Kartouni, D. Delahaye. "Characterization of Copper Oxidation by Linear Potential Sweep Voltammetry and UV-Visible-NIR Diffuse Reflectance Spectroscopy". J. Appl. Electrochem. 1991. 21(8): 697–702.
29. S.R. De Sánchez, L.E.A. Berlouis, D.J. Schiffrin. "Difference Reflectance Spectroscopy of Anodic Films on Copper and Copper Base Alloys". J. Electroanal. Chem. Interfacial Electrochem. 1991. 307(1–2): 73–86.
30. S. Pratesi, M. De Lucia, M. Meucci, E. Sani. "Structural and Optical Properties of Copper-Coated Substrates for Solar Thermal Absorbers". Superlattices Microstruct. 2016. 98: 342–350.
31. P.B. Johnson, R.W. Christy. "Optical Constants of the Noble Metals". Phys. Rev. B. 1972. 6(12): 4370–4379.
32. P.E. Ciddor. "Refractive Index of Air: New Equations for the Visible and Near Infrared". Appl. Opt. 1996. 35(9): 1566.
33. F.K. Mugwang'a, P.K. Karimi, W.K. Njoroge, O. Omayio, et al. "Optical Characterization of Copper Oxide Thin Films Prepared by Reactive DC Magnetron Sputtering for Solar Cell Applications". Int. J. Thin Film. Sci. Technol. 2013. 2(1): 12–24.
34. B. Maack, N. Nilius. "Oxidation of Polycrystalline Copper Films–Pressure and Temperature Dependence". Thin Solid Films. 2018. 651: 24–30.
35. Y.Z. Hu, R. Sharangpani, S.-P. Tay. "Kinetic Investigation of Copper Film Oxidation by Spectroscopic Ellipsometry and Reflectometry". J. Vac. Sci. Tech. 2000. 18(5): 2527.
36. A. Musa, T. Akomolafe, M. Carter. "Production of Cuprous Oxide, a Solar Cell Material, by Thermal Oxidation and a Study of Its Physical and Electrical Properties". Sol. Energy Mater. Sol. Cells. 1998. 51(3–4): 305–316.
37. P.J.M. Isherwood, J.M. Walls. "Cupric Oxide-Based P-Type Transparent Conductors". Energy Procedia. 2014. 60: 129–134.
38. O. Messaoudi, H. Makhlouf, A. Souissi, I. Ben Assaker, et al. "Correlation Between Optical and Structural Properties of Copper Oxide Electrodeposited on ITO Glass". J. Alloys Compd. 2014. 611: 142–148.
39. N. Khaorapapong, N. Khumchoo, M. Ogawa. "Preparation of Copper Oxide in Smectites". Appl. Clay Sci. 2015. 104: 238–244.
40. B. Timmermans, F. Reniers, A. Hubin, C. Buess-Herman. "Chemical Effects in the Auger Spectrum of Copper–Oxygen Compounds". Appl. Surf. Sci. 1999. 144–145: 54–58.
41. H. Bubert, M. Korte, R.P.H. Garten, E. Grallath, et al. "Application of Factor Analysis in Electron Spectroscopic Depth Profiling on Copper Oxide". Anal. Chim. Acta. 1994. 297(1–2): 187–195.
42. D.B. Yang, D. Wolf. "Interfacial Analyses of Copper Corrosion by Acrylic and Methacrylic Acids Using XPS, Auger and Grazing Angle FTIR Spectroscopy". Surf. Interface Anal. 1995. 23(5): 276–288.
43. Y. Yu, K. Sagisaka, D. Fujita. "Surface Segregation of Aluminum Atoms on Cu-9 At.% Al(1 1 1) Studied by Auger Electron Spectroscopy and Low Energy Electron Diffraction". Surf. Sci. 2009. 603(4): 723–726.
44. S.R. Barman, D.D. Sarma. "Investigation of the L3-M45M45 Auger-Spectra of Cu, Cu_2O and CuO". J. Phys. Condens. Matter. 1992. 4(37): 7607–7616.
45. E. Takano, T. Mino, K. Takahashi, K. Sawada, et al. "The Oxidation Control of Copper Leadframe Package for Prevention of Popcorn Cracking". Proceedings of the 47th Electronic Components and Technology Conference. San Jose, CA; 18–21 May, 1997.
46. K.F. Kusano, M. Uchikoshi, K. Mimura, M. Isshiki. "Low-Temperature Oxidation of Cu(100), Cu(110) and Cu(111)". Oxid. Met. 2014. 82(3–4): 181–193.
47. S.J. Cho, K.W. Paik. "Oxidation Studies on a Cu-Base Leadframe Alloy Between 150 °C and 300 °C". Scr. Mater. 1998. 38(7): 1149–1154.
48. H. Zhan, J. Fang, L. Tang, H. Yang, et al. "Application of Near-Infrared Spectroscopy for the Rapid Quality Assessment of Radix Paeoniae Rubra". Spectrochim. Acta, Part A. 2017. 183: 75–83.
49. X. Yin, Y. Li, F. Ke, C. Lin, et al. "Evolution of the Raman Spectrum of Graphene Grown on Copper Upon Oxidation of the Substrate". Nano Res. 2014. 7(11): 1613–1622.
50. B. Purusottam-Reddy, K. Sivajee-Ganesh, K. Jayanth-Babu, O.M. Hussain, et al. "Microstructure and Supercapacitive Properties of RF-Sputtered Copper Oxide Thin Films: Influence of O_2/Ar Ratio". Ionics. 2015. 21(8): 2319–2328.
51. A.G. Christy, A. Lowe, V. Otieno-Alego, M. Stoll, et al. "Voltammetric and Raman Microspectroscopic Studies on Artificial Copper Pits Grown in Simulated Potable Water". J. Appl. Electrochem. 2004. 34(2): 225–233.
52. C. Baratto, R. Kumar, G. Faglia, K. Vojisavljević, et al. "P-Type Copper Aluminum Oxide Thin Films for Gas-Sensing Applications". Sens. Actuators B. 2015. 209: 287–296.